JOURNAL OF MATERIALS SCIENCE **40** (2005) 5273–5280

Effect of combined doping ($y^{3+} + fe^{3+}$) on structural features of nanodispersed zirconium oxide

A. G. BELOUS, E. V.PASHKOVA, O. I. V'YUNOV
V.I.Vernadskii Institute of General and Inorganic Chemistry, Kyiv, Ukraine

V. P. IVANITSKII
Institute of Geochemistry, Mineralogy and Ore Formation, Kyiv, Ukraine

Fully stabilized zirconium dioxide is widely used. One of the basic requirements to this material is the thermal stability of the structure. The most effective stabilizer for zirconium oxide is yttrium oxide. However, the structure of Y-ZrO_2 degraded at low temperature. Partial substitution of Fe^{3+} for Y^{3+} decreases both the crystallization and sintering temperature of zirconia ceramic.

The aim of present work is the investigation of structural peculiarities of zirconium oxide stabilized by combined dopant depending on chemical composition, synthesis conditions and heat treatment.

The polymorphic composition of a ZrO_2-based materials has been determined in series of samples that correspond to the formula $[1-(x+y)]ZrO_2 \cdot xY_2O_3 \cdot yFe_2O_3$ in the temperature range 620–1570 K. It has been found that at the same molar ratio ZrO_2 : doping oxides, the degree of ZrO_2 stabilization increases, and the low-temperature degradation process is retarded by the partial substitution of Fe^{3+} for Y^{3+}. Nonequivalent sites of Fe^{3+} ions have been identified: two with octahedral coordination for CPH and three with octa-, penta- and tetrahedral coordination for SPH. The possibility of cluster distribution of Fe^{3+} ions and the dependence of the number of vacancies on synthesis conditions have been shown.

1. Introduction

Yttrium oxide is the most efficient and commonly used stabilizer of high-temperature zirconium dioxide modifications [1–3]. However, the structure of yttrium-stabilized ZrO_2 is susceptible to low-temperature degradation, which is caused by tetragonal-monoclinic transformation [4, 5]. Therefore, the search for new stabilizers and modification of them are a topical problem. The choice of iron oxide as the third component of the system ZrO_2-Y_2O_3-Fe_2O_3 is dictated both by steric factors and by the possibility to lower the crystallization [6] and sintering [7] temperatures of ZrO_2-based solid solutions. Lowering the above temperatures facilitates production of fine ZrO_2 powders and realization of fine-grain microstructure, which is the most important condition for producing high-strength ceramics.

The ratio of the monoclinic (m), tetragonal (t), and cubic (c) polymorphic modifications of ZrO_2 and their structure features are known to determine the mechanical and electrophysical properties and the application range of ZrO_2 ceramic [8].

The aim of the work is to investigate the structure features (polymorphic composition, positions of ions, site occupancies, local environment of Fe^{3+} ions) of zirconium dioxide stabilized by a complex dopant (Y_2O_3 and Fe_2O_3) as a function of the chemical composition of samples and their precipitation, heat treatment, and ageing conditions.

2. Experimental procedure

Samples for investigation were prepared by calcining $ZrO(OH)_2$-$Y(OH)_3$-FeOOH hydroxides precipitated from concentrated solutions of $ZrOCl_2$, $Y(NO_3)_3$, and $Fe(NO_3)_3$ with an ammonia solution by two methods: coprecipitation (CPH) and sequential precipitation (SPH). Using the SPH method, $Y(OH)_3$ was precipitated on coprecipitated $ZrO(OH)_2$and FeOOH. The precipitates were washed to remove Cl^- and NO_3^- ions, and dried at 350 K. Heat treatment was performed in a chamber furnace at 970–1470 K. Compositions corresponding to the formula $[1-(x+y)]ZrO_2 \cdot xY_2O_3 \cdot yFe_2O_3$, where $x = 0$, 0.01, 0.015, 0.02, 0.03 and $x + y = 0.03$ (*series I*); $x = y = 0.02$, 0.025, 0.03, 0.04 and $x + y > 0.03$ (*series II*). The samples were investigated just after heat treatment and after storing them in air for three years. The investigations were carried out using chemical and X-ray analysis, atomic absorption spectroscopy, Mössbauer spectroscopy (MS), and electron microscopy. The X-ray

0022–2461
DOI: 10.1007/s10853-005-0842-1

investigations were carried out on a DRON 4-07 diffractometer (Cu K_α radiation, 40 kV, 20 mA, step-scan mode with a step size $\Delta 2\Theta = 0.02^\circ$ and a counting time per data point of 6 s). Data were collected over an angle range of $2\Theta = 10$–150°. SiO_2 (2Θ standard) and NIST SRM 1976 – Al_2O_3 (certified intensity standard [9]) were used as external standards. The full width at half-maxima (FWHM) β of the profile was used to determine the lattice microstrain η and the coherent scattering area D, using the so-called Hall equation $\beta \cdot \cos\Theta = K \cdot \lambda / D + 2 \cdot \eta \cdot \sin\Theta$, where Θ is the Bragg angle of diffraction, K the shape factor (a value of 0.95 was used in this study), and λ the X-ray wavelength.

The cubic, tetragonal and monoclinic phase content was determined from the equations [10]:

$$C_m = \frac{I_m(111) + I_m(11\,\bar{1})}{I_m(111) + I_m(11\,1) + I_c(111) + I_t(101)} \times 100\% \quad (1)$$

$$\frac{C_m}{C_t + C_c} = 0.82 \frac{I_m(111) + I_m(11\,\bar{1})}{I_c(111) + I_t(101)} \times 100\% \quad (2)$$

$$\frac{C_c}{C_t} = 0.88 \frac{I_c(400)}{I_t(400) + I_t(220)} \times 100\% \quad (3)$$

$$C_m + C_t + C_c = 100\% \quad (4)$$

where C is the volume fraction of corresponding phase, and I is the intensity of reflection, given in brackets. The legitimacy of using calculations from the above equations to establish the polymorphic composition of stabilized zirconium dioxide was verified on artificial mixtures of m-, t- and c-ZrO_2 of known composition. Single-phase samples with m-, t- and c structure were obtained for the compositions $0.99ZrO_2 \cdot 0.01Y_2O_3$, $0.94ZrO_2 \cdot 0.06Y_2O_3$ and $0.92ZrO_2 \cdot 0.08Y_2O_3$ respectively. The error of determination of m-ZrO_2 content was 1.5–2% and that of t- and c-ZrO_2 content 3.5–4%.

Mössbauer spectra were obtained by using an electrodynamic spectrometer which operates in the constant-acceleration mode with a ^{57}Co γ-quantum source in Rh matrix. The measurements were made at room temperature. The calibrations of the velocity scale in the magnetic and paramagnetic measurement ranges were performed by means of α-Fe and sodium nitroprusside respectively (to reduce the isomer shift values, given with relative to α-Fe, to isomer shifts relative to sodium nitroprusside, 0.258 mm/s must be added to the first value). The isomer shifts for the spectra of each of the ranges (V) were given with respect to the calibrations used. The spectra were processed using a program that realizes the least-squares method.

The iron content was determined on a Pye Unicom SP 9 atomic absorption spectrometer ($\lambda = 248.3$ nm, slit width 0.2 nm, flame: acetone–air). Zirconium and yttrium were determined according to a "fluoride scheme" [11]. Besides, the zirconium content was determined by the method described in Ref [12].

The micrographs were taken on a JEOL JEM 100 CX II electron microscope. The samples were prepared by dispersing powder in acetone (5 min). A drop of dispersion was applied to a carbon film.

3. Results and discussion

The results of a chemical analysis of series I and II samples, which are listed in Table I, support the correspondence of the actual composition to the predetermined one (within the error of analyses).

According to XRD analysis, c-ZrO_2 of $0.97ZrO_2 \cdot 0.03Y_2O_3$ samples crystallizes at 770 K, and that of $0.97ZrO_2 \cdot 0.015Y_2O_3 \cdot 0.015Fe_2O_3$ crystallizes at 620 K (Fig. 1, curves 1). The decrease in c-ZrO_2crystallization temperature on partial substitution of $Fe_2O_3$for Y_2O_3 may be due to the fact that less thermally stable iron hydroxide makes for lower dehydration temperature of zirconium and yttrium hydroxides [13] and hence aids the crystallization of stabilized zirconium dioxide. Raising the heat treatment temperature to over 770–870 K causes a tetragonal distortion of cubic unit cell, as evidenced by a splitting of the diffraction reflections 200 and 311, as well as by the formation of monoclinic ZrO_2 modification. In this case, the diffractograms of the series I samples exhibit at $x = 0.015$, 0.02 and 0.03 three ZrO_2 modifications: $c + t + m$, and at $x = 0.01c + t + m+$ traces of $\alpha\alpha$-Fe_2O_3 (Fig. 1,

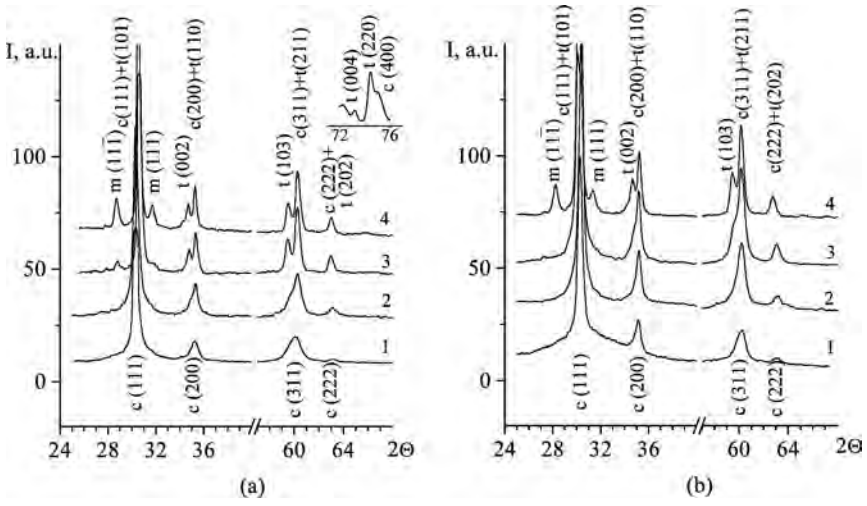

Figure 1 X-ray powder diffractograms of $0.97ZrO_2 \cdot 0.03Y_2O_3$ (a) and $0.97ZrO_2 \cdot 0.015Y_2O_3 \cdot 0.015Fe_2O_3$(b) samples.

TABLE I Results of a chemical analysis of $[1-(x+y)]ZrO_2 \cdot xY_2O_3 \cdot yFe_2O_3$ samples heat-treated at $T = 1270$ K (CPH and SPH)

No	Nominal composition	Oxide to be determined	Chemical composition, wt%		
				Actual	
			Predeter-mined	CPH	SPH
		Series I ($x + y = 0.03$)			
1.	$0.97ZrO_2 \cdot 0.03Fe_2O_3$	ZrO_2	96.15	96.30	96.21
	$Zr_{0.942}Fe_{0.058}O_{1.977}$	ZrO_2^*		96.09	96.11
		Fe_2O_3	3.85	3.71	3.76
2.	$0.97ZrO_2 \cdot 0.01Y_2O_3 \cdot 0.02Fe_2O_3$	ZrO_2	95.64	95.87	95.87
	$Zr_{0.942}Y_{0.019}Fe_{0.039}O_{1.977}$	ZrO_2^*		95.49	95.45
		Y_2O_3	1.81	1.82	1.85
		Fe_2O_3	2.55	2.48	2.50
3.	$0.97ZrO_2 \cdot 0.02Y_2O_3 \cdot 0.01Fe_2O_3$	ZrO_2	95.13	95.27	95.29
	$Zr_{0.942}Y_{0.039}Fe_{0.019}O_{1.977}$	ZrO_2^*		95.15	–
		Y_2O_3	3.60	3.65	3.62
		Fe_2O_3	1.27	1.31	1.26
4.	$0.97ZrO_2 \cdot 0.03Y_2O_3$	ZrO_2	94.64	94.72	94.75
	$Zr_{0.942}Y_{0.058}O_{1.977}$	ZrO_2^*		94.60	94.58
		Y_2O_3	5.36	5.32	5.32
		Series II ($x + y > 0.03$)			
5.	$0.96ZrO_2 \cdot 0.02Y_2O_3 \cdot 0.02Fe_2O_3$	ZrO_2	93.88	93.91	93.95
	$Zr_{0.924}Y_{0.038}Fe_{0.038}O_{1.962}$	Y_2O_3	3.59	3.61	3.59
		Fe_2O_3	2.53	2.43	2.50
6.	$0.94ZrO_2 \cdot 0.03Y_2O_3 \cdot 0.03Fe_2O_3$	ZrO_2	90.92	91.20	91.20
	$Zr_{0.886}Y_{0.057}Fe_{0.057}O_{1.943}$	ZrO_2^*		90.70	90.70
		Y_2O_3	5.31	5.31	5.30
		Fe_2O_3	3.76	3.60	3.62
7.	$0.92ZrO_2 \cdot 0.04Y_2O_3 \cdot 0.04Fe_2O_3$	ZrO_2	88.03	88.13	88.21
	$Zr_{0.852}Y_{0.074}Fe_{0.074}O_{1.926}$	Y_2O_3	7.01	6.93	7.12
		Fe_2O_3	4.96	4.81	4.87

Note: ZrO_2, determination by the procedure reported in [11]; ZrO_2^*, determination by the procedure reported in [12].

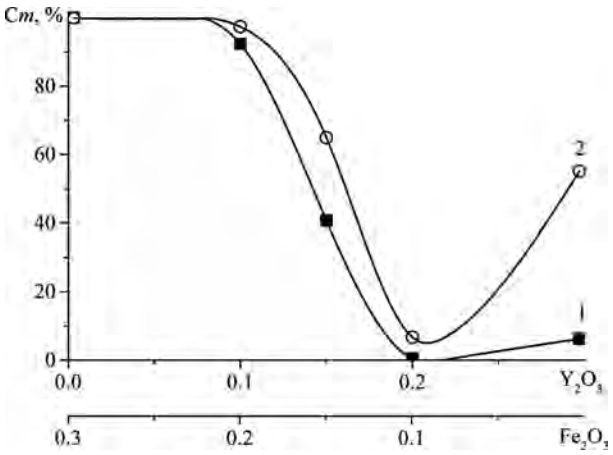

Figure 2 Monoclinic ZrO_2 modification content of $0.97ZrO_2 \cdot x Y_2O_3 \cdot yFe_2O_3$ samples as a function of the x:y ratio: (1) CPH, (2) SPH.

curves 3–5). Cubic and tetragonal modifications were distinguished within 2Θ range of 73–75° (Fig. 1, insertion).

Fig. 2 shows the concentration dependence of the percentage of monoclinic modification C_m in series I samples for different methods of precipitation of hydroxides after heat treatment at 1470 K, and Fig. 3 shows the temperature dependence of C_m of series I samples for different hydroxide precipitation methods and x:y ratios in as-fired samples and after storage for 3 years. The optimal stabilization of zirconium dioxide for the compositions under study is observed at the ratio Y_2O_3:$Fe_2O_3 = 0.02$:0.01. The degree of stabilization at this ratio is higher than for the samples in which only Y_2O_3 was used as stabilizer (Figs 2 and 3, curves 3, 4).

It follows from Figs 2 and 3 (curve 1) that these is practically no stabilization of the high-temperature c and t modifications of ZrO_2 in the temperature range 1170–1570 K in the case of the complete substitution of Fe_2O_3 for Y_2O_3. The stabilizing effect of Fe_2O_3 on the structure of ZrO_2 at the above temperatures manifests itself only when it is present together with Y_2O_3 (Figs 2 and 3, curves 2–4).

Fe_2O_3 also has a wholesome effect on the phase stability of ZrO_2 in time. During storage, zirconium dioxide powders are subject to t-$ZrO_2 \rightarrow m$-ZrO_2transformations [14]. The results given in Fig. 3 indicate that the process of low-temperature degradation of zirconium dioxide in the ternary system $0.97ZrO_2 \cdot xY_2O_3 \cdot yFe_2O_3$(curves 3–3′) is slower than in the binary system $0.97ZrO_2$-$0.03Y_2O_3$ (curves 4–4′).

The analysis of the polymorphic composition of samples I (Fig. 3) shows that the method of hydroxide precipitation (CPH or SPH) affects greatly the degree of ZrO_2 stabilization, especially for samples after thermal treatment at $T > 1270$ K. Under sequential precipitation conditions (Fig. 3b), the degree of ZrO_2 stabilization is much lower as compared with CPH (Fig. 3a) for all x:y ratios (curves 1–4), except the ratio x:$y = 0.02$:0.01 (curve 3). Recently we shown that soft, readily destructible aggregates are formed on heat treatment of sequentially precipitated hydroxides (in contrast to

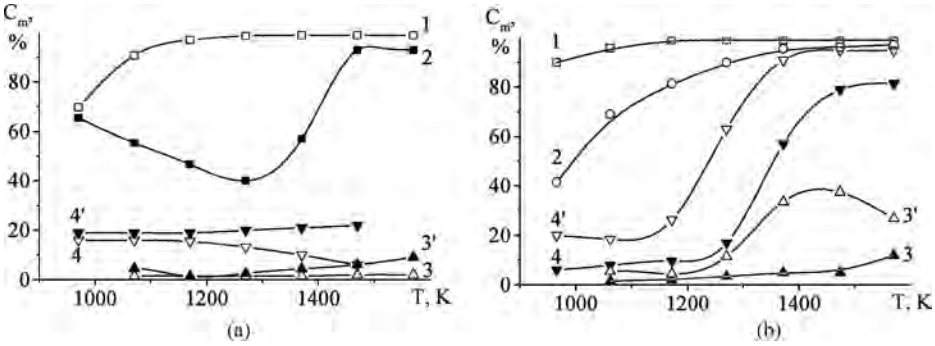

Figure 3 Monoclinic ZrO_2 modification content of $0.97ZrO_2 \cdot xY_2O_3 \cdot yFe_2O_3$ samples ($x + y = 0.03$) as a function of heat treatment temperature: (a) CPH, (b) SPH; $x = 0$ (1); 0.01 (2); 0.02 (3); 0.03 (4)—as-heat-treated samples; $x = 0.02$ (3′); 0.03 (4′)—after storage in air for 3 years.

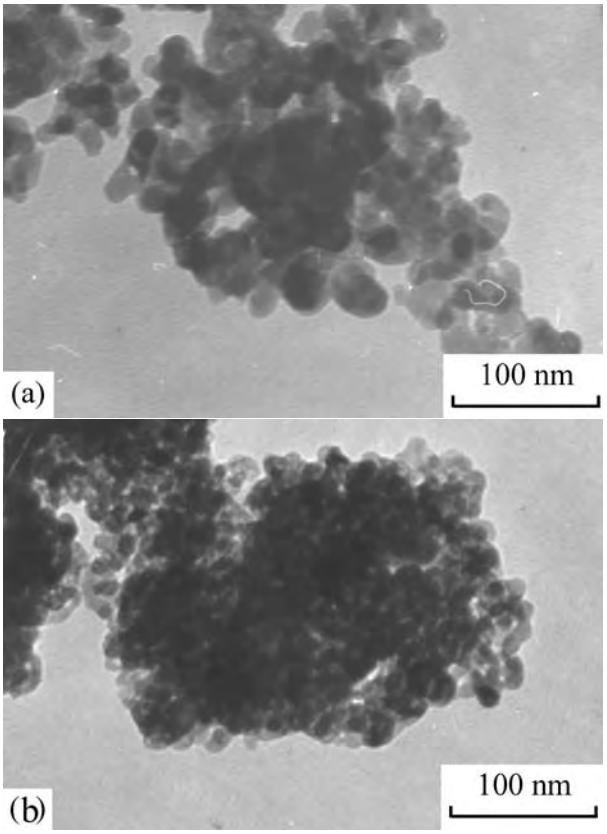

Figure 4 Microstructure of $Zr_{0.886}Y_{0.057}Fe_{0.057}O_{2-\delta}$ samples heat-treated at 870 K: (a) CPH, (b) SPH.

coprecipitated hydroxides) [14], making it possible to produce fine ZrO_2 powders with a particle size of 10–20 nm (Fig. 4) without disaggregation and/or milling. Therefore, it is important to determine the composition of the samples obtained by sequential precipitation, in which a high degree of stabilization and friability of powders are retained on heat treatment. The transformation t-$ZrO_2 \rightarrow m$-ZrO_2 during the ageing of the samples obtained by coprecipitation proceeds much more slowly than in the sequentially precipitated samples (Fig. 3, curves 3, 3′ and 4, 4′).

Fig. 5 shows the polymorphic composition of samples II as a function of hydroxide precipitation conditions, heat treatment temperature and chemical composition. In the samples under investigation there is a small amount of α-Fe_2O_3, which does not practically vary with x and y, therefore the α-Fe_2O_3 phase was not taken into account (Fig. 6, the α-Fe_2O_3 phase is denoted by arrows). It is seen from Fig. 5 that the regions of the c-ZrO_2 and $(c + t)$-ZrO_2 phases enlarge with increasing amount of doping oxides $(x + y)$. For the compositions with $x = y = 0.02$, 0.025 and 0.03, a small amount of $m-ZrO_2$ appears, in addition to $(c + t)$-ZrO_2, at temperatures above 1070, 1170 and 1200 K respectively (Fig. 3a–c). For the compositions with $x = y = 0.04$, the complete stabilization of ZrO_2 takes place within studied temperature range (Fig. 3d). When comparing the monoclinic ZrO_2 modification contents of samples with the same molar ratio ZrO_2: doping oxide ($0.96ZrO_2 \cdot 0.04Y_2O_3$ [14] and $0.96ZrO_2 \cdot 0.02Y_2O_3 \cdot 0.02Fe_2O_3$) (Fig. 3a), it is evident that the degree of ZrO_2stabilization increases greatly on the partial substitution of Fe_2O_3 for Y_2O_3. Since for the composition $0.94ZrO_2 \cdot 0.03Y_2O_3 \cdot 0.03Fe_2O_3$ ($Zr_{0.886}Y_{0.057}Fe_{0.057}O_{2-\delta}$) complete stabilization of zirconium dioxide is observed at 1470 K for both methods of hydroxide precipitation (CPH and SPH), the above samples were chosen for the investigation of the local environment of Fe^{3+} ions by MS. X-ray investigations showed these samples (CPH and SPH) to have a CaF_2-type structure with tetragonal distortion of lattice (space group $P4_2/nmc$ (137)) (Fig. 6, Table II). It should be noted that for simplicity the unit cell parameters of the tetragonal form have often described in the terms of face-centered symmetry in order to relate it to the face-centered CaF_2 structure [15, 16]. The absence of other modifications (c and m-ZrO_2) from them will make it possible to exclude the ambiguity of interpretation of MS's.

The MS's obtained in the magnetic range are shown in Fig. 7, and their parameters are listed in Table III. The spectra of both (CPH and SPH) samples are represented by a superposition of a Zeeman splitting sextet, whose parameters agree with those published for hematite [17, 18], and a quadrupole splitting doublet, whose parameters are characteristic of high-spin Fe^{3+} ions in octahedral coordination. The parameter values of the α-Fe_2O_3 sextet are close to those for bulk magnetically ordered hematite, indicating that there is no noticeable solubility of other cations of the system in the hematite structure. Such substitutions are generally accompanied by a decrease in the values of effective magnetic field on iron nuclei (H_{eff}). The asymmetric character of absorption lines may be due to the presence

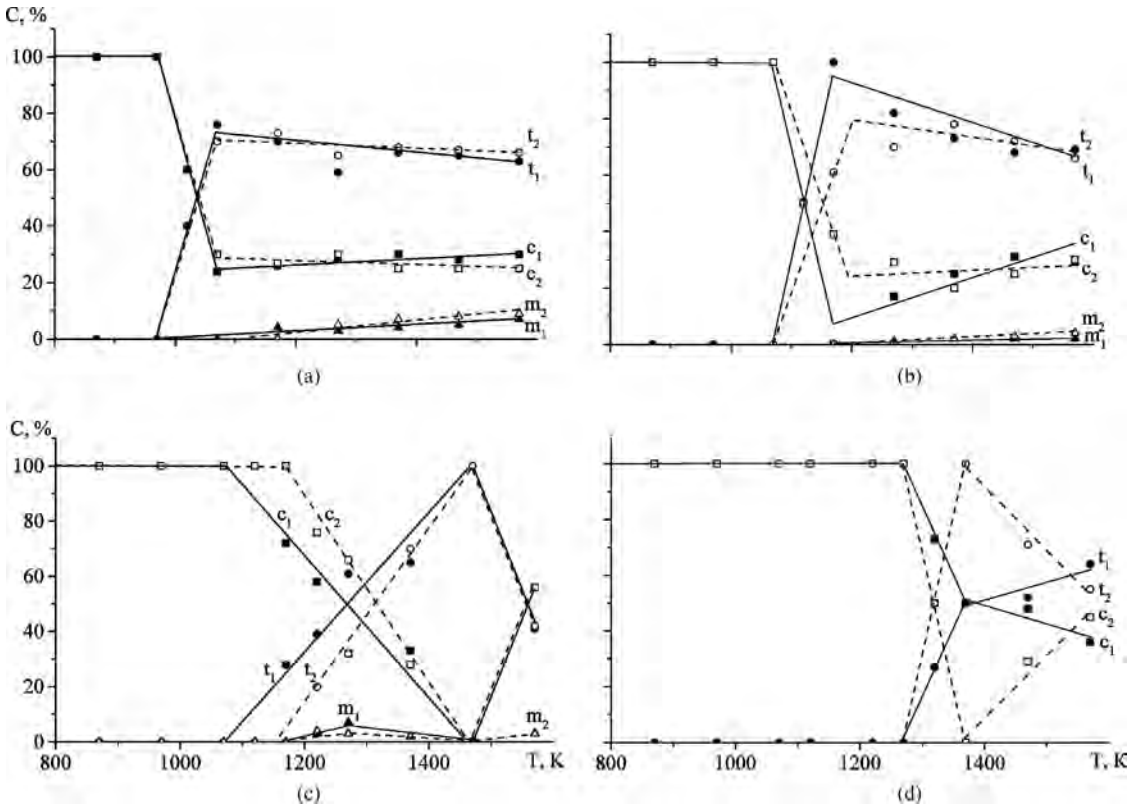

Figure 5 Polymorphic composition of stabilized zirconium dioxide [1-($x + y$)]$ZrO_2 \cdot xY_2O_3 \cdot yFe_2O_3$ ($x + y > 0.03$) as a function of heat treatment temperature: $x = y = 0.02$ (a); 0.025 (b); 0.03 (c) and 0.04 (d); c_1, t_1, m_1: CPH, c_2, t_2, m_2: SPH.

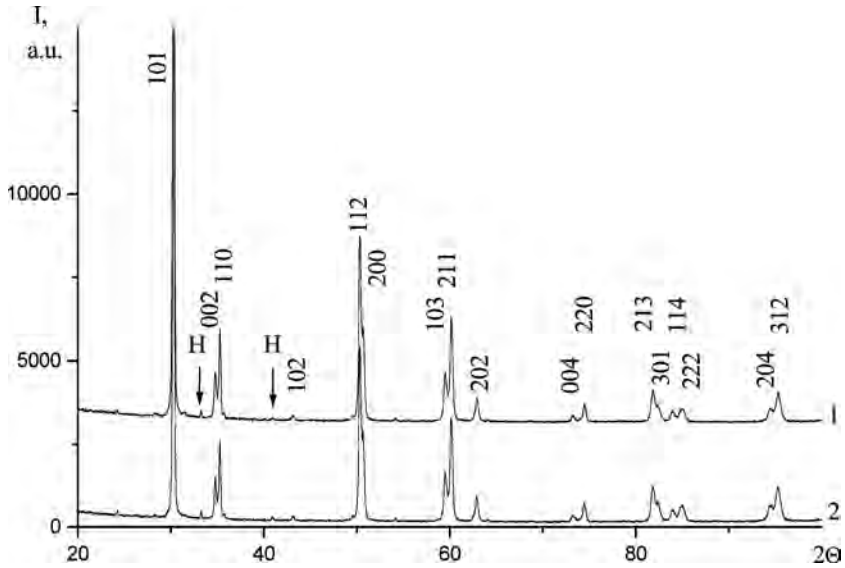

Figure 6 X-ray powder diffractograms of $Zr_{0.886}Y_{0.057}Fe_{0.057}O_{2-\delta}$ samples: (1) CPH, (2) SPH.

of several nonequivalent sites of Fe^{3+} ions and the high values of absorption line FWHM to the inhomogeneity of the cation environment of Fe^{3+} ions. The procedure for the mathematical separation of lines, which are a superposition of several components, which are less than FWHM value apart, is incorrect, as shown in Ref. [19], which excludes their unambiguous interpretation.

To reduce experimental errors and to explain the character of the asymmetry of the doublet lines, we have obtained spectra in the paramagnetic measurement range, the resolvability of the spectra in which is more than three times as high as in the magnetic range. This allowed us to interpret in greater detail the structure of the Fe^{3+} doublets (Fig. 8). The parameters of the resolved components of spectra are listed in Table IV. In the spectra of the samples under investigation, two external lines are well resolvable; their centers are on the velocity scale at –0.56 and 2.05 mm/s, which corresponds to the positions of the internal third and fourth lines of the Zeeman splitting sextet of hematite (Fig. 7). For convenience in spectrum separation and subsequent calculations of relative contributions of the components to the overall spectrum, these two lines are represented by a quadrupole splitting doublet with lines that are

TABLE II Structural parameters of solid solutions $Zr_{0.886}Y_{0.057}Fe_{0.057}O_{2-\delta}$ prepared by CPH and SPH (T = 1270 K, 2 h)

$P4_2/nmc$ (137)	CPH	SPH
	Unit cell parameters	
a(Å)	3.60567(9)	3.60628(9)
c(Å)	5.1694(2)	5.1690(2)
V (Å^3)	67.206(3)	67.224(3)
$c/\sqrt{2}a$	1.013(1)	1.013(1)
	Positions of atoms	
O: z	0.467(1)	0.465(1)
	Interatomic distances	
<Zr-O>	2.22	2.22
	Temperature factors (Å^2)	
Zr	0.90(2)	0.08(2)
Y	0.90(2)	0.08(2)
Fe	0.90(2)	0.08(2)
O	2.2(2)	2.1(1)
	Site occupancies	
Zr	0.926	0.925
Y	0.058	0.058
Fe	0.016	0.017
O	1.80(2)	1.87(3)
	Agreement factors	
R_B (%)	2.30	3.19
R_f (%)	2.73	2.33
	Lattice microstrains	
η, %	8.7(1)	9.6(1)

Note: Positions of atoms: Zr 2a (3/4 1/4 3/4), O 4d (1/4 1/4 z); R_B = Bregg factor; R_f = form factor.

TABLE III Parameters of Mössbauer spectra of $Zr_{0.886}Y_{0.057}Fe_{0.057}O_{2-\delta}$ samples obtained in the magnetic measurement range

Sample	Phase, ion	H_{eff} (kOe)	IS (mm/s)	QS (mm/s)	FWHM (mm/s)	S (%)
1 (CPH)	Hematite	514	0.38	0.22	0.36	70.3
	Fe^{3+}_{paramag}	0	0.33	1.07	0.86	29.7
2 (SPH)	Hematite	515	0.37	0.23	0.32	68.3
	Fe^{3+}_{paramag}	0	0.37	1.08	0.90	31.7

Note: $Fe^{3+}_{\text{paramag}} = Fe^{3+}$ in paramagnetic state; H_{eff} = effective magnetic field; IS = isomer shift relative to α-Fe, QS = quadrupole splitting; FWHM = absorption line full width at half-maxima; S = relative area of component. Measurement error of IS, QS and FWHM: ± 0.04 mm/s, H_{eff}: ± 5 kOe, S :≤10 %.

described by equal values of intensities and FWHM. The iron content of each component was determined from their areas proceeding on the assumption that the Fe^{3+} resonance absorption coefficients are equal in all coexisting structure sites, and that the intensities of the hematite sextet lines obey the ratio 3:2:1:1:2:3. The area of the internal third and fourth lines of the sextet, which can be seen in Fig. 7, is ca. 1/6 of its total area. By multiplying the values obtained of the relative area of the components (S) of the internal hematite lines by six and adding this product to the areas of the paramagnetic components, we obtain the values of the area that corresponds to the resonance absorption of gamma quanta on the nuclei of all Fe^{3+} ions that are contained in samples. The relative contribution of each MS component (S_o, %) was calculated from this sum (Table IV). As is obvious from comparison of the data given in Tables III and IV, the contributions of the magnetic component

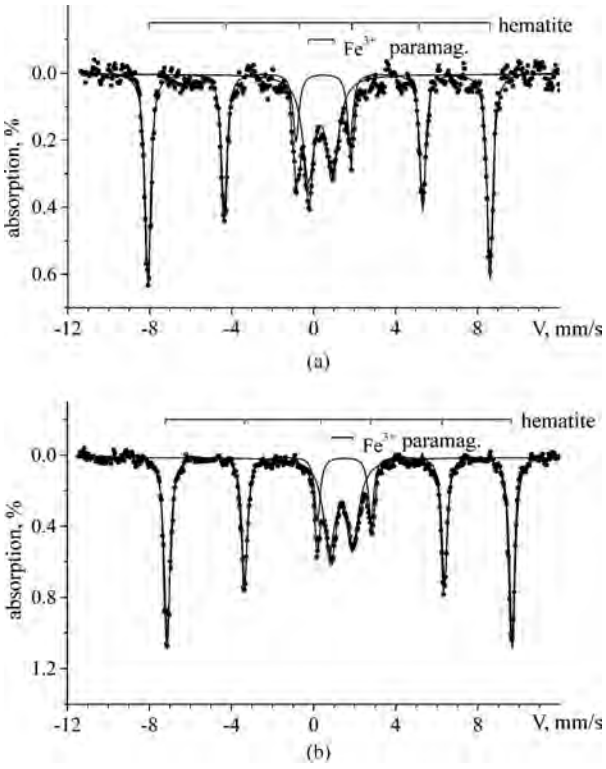

Figure 7 Mössbauer spectra of $Zr_{0.886}Y_{0.057}Fe_{0.057}O_{2-\delta}$ samples obtained in the magnetic measurement range: (a) CPH, (b) SPH.

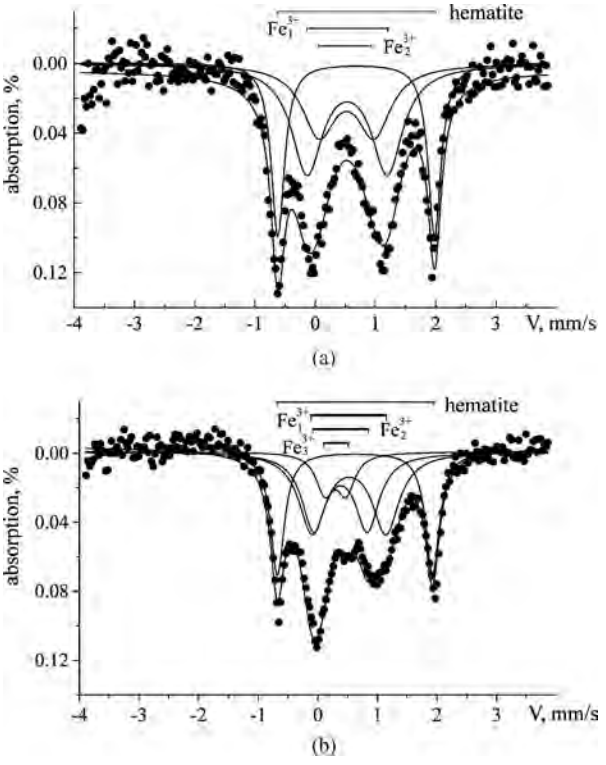

Figure 8 Mössbauer spectra of $Zr_{0.886}Y_{0.057}Fe_{0.057}O_{2-\delta}$ samples obtained in the paramagnetic measurement range: (a) CPH, (b) SPH.

and the sum of the paramagnetic components of Fe^{3+} do not change for both samples within experimental errors on changeover from one measurement scale to another.

The visually recognizable features of the internal spectral lines (Fig. 8) (asymmetry of the lines in intensity and width and of their bends) allowed us to

TABLE IV Parameters of Mössbauer spectra of $Zr_{0.886}Y_{0.057}Fe_{0.057}O_{2-\delta}$ samples obtained in the paramagnetic measurement range

Sample	Phase, ion	IS (mm/s)	QS (mm/s)	FWHM (mm/s)	S (%)	S_o (%)
1 (CPH)	Hematite	0.76	2.60	0.27	30.5	72.5
	Fe_1^{3+}	0.64	1.33	0.54	42.0	16.6
	Fe_2^{3+}	0.63	0.84	0.53	27.5	10.9
2 (SPH)	Hematite	0.75	2.60	0.25	26.6	68.5
	Fe_1^{3+}	0.66	1.21	0.55	36.5	15.7
	Fe_2^{3+}	0.52	0.92	0.46	26.2	11.2
	Fe_3^{3+}	0.43	0.40	0.37	10.7	4.6
2*(SPH)	Hematite	0.75	2.61	0.29	29.8	71.8
	Fe_1^{3+}	0.66	1.18	0.52	34.0	13.7
	Fe_2^{3+}	0.49	0.94	0.62	26.4	10.6
	Fe_3^{3+}	0.40	0.44	0.42	9.8	3.9

Note: The symbols are the same as in Table III. S_o = area of component reduced with respect to the six-line spectrum of hematite. IS's have been reduced with respect to sodium nitroprusside. Measurement error IS, QS and FWHM: ±0.03 mm/s, S: ≤10%. 2*: the sample has been kept in air for three years.

distinguish two doublets due to Fe_1^{3+} and Fe_2^{3+} in the spectra of samples obtained by CPH and three doublets due to Fe_1^{3+}, Fe_2^{3+} and Fe_3^{3+} in the spectra of samples obtained by SPH. It follows from Table IV that ≈30% of the introduced quantity of iron dissolves as Fe^{3+} in the tetragonal zirconium dioxide samples under investigations. About ≈70 Fe^{3+} is required for the formation of the α-Fe_2O_3 phase.

The results presented in Fig. 8 and in Table IV make it possible to identify in the solid solutions $Zr_{0.886}Y_{0.057}Fe_{0.057}O_{2-\delta}$ obtained by CPH and SPH two and three nonequivalent sites of Fe^{3+} ions, respectively, in accordance with the number of resolved doublets. It is obvious that the different variants of the arrangement of vacancies in the first coordination sphere and Zr, Y and Fe cations in the second coordination sphere as well as of their quantitative ratios give rise to the formation of a nonequivalent environment of Fe^{3+} ions.

As follows from Table IV, the MS parameters of samples obtained by SPH do not practically change after air storage for three years (samples 2 and 2*). This indicates the absence or considerable retardation of the low-temperature degradation of the zirconium dioxide structure in the ZrO_2-Y_2O_3-Fe_2O_3 system in comparison with the binary ZrO_2-Y_2O_3 system [14].

When interpreting MS's, the value of quadrupole splitting (QS) may be taken as a measure of distortion of coordination polyhedra and deviation of their symmetry from cubic symmetry. Each change in the distortions of coordination polyhedra results in corresponding variations of QS. The value of isomer shift (IS) may be associated with the coordination of Fe^{3+} ions. According to [20, 21], decrease (increase) in the coordination number (CN) of resonance ions usually leads to a decrease (increase) in IS values, which is due to an increase (decrease) in covalent bond via 4s orbitals owing to a decrease (increase) in cation-oxygen distance. The unsuitability for Fe^{3+} of the coordination with the coordination number of 8, which is peculiar to the host Zr^{4+}cation in tetragonal and cubic ZrO_2, is associated with the smaller ionic radius of Fe^{3+}_{CN6} (0.0645 nm) as compared to Zr^{4+} (0.084 nm) [22] and with the tendency of crystal lattice to electroneutrality. The negative lattice charge is neutralized, in the case of the $2Zr^{4+} \rightarrow 2Fe^{3+}$substitution, by the removal of one O^{2-} ion from the anion polyhedron. The decrease in interatomic distances in the oxygen polyhedron on the partial substitution of Fe^{3+} for Y^{3+} ions ($R_{Fe^{3+}CN6} = 0.06457$ nm, $R_{Y^{3+}CN6} = 0.1015$ nm) [22] enhances the electrostatic repulsion of oxygen ions [23], which facilitates the formation of octahedral coordination of Fe^{3+} ions.

Taking into account the results of [23, 24], where clusters were found using high-resolution electron microscopy, the presence of several doublets in the MS's of $Zr_{0.886}Y_{0.057}Fe_{0.057}O_{2-\delta}$samples with different values of their areas (Table IV) may be attributed to the cluster character of iron distribution in the solid solution ZrO_2-Y_2O_3-Fe_2O_3. In the opinion of the authors of [25], this distribution is typical of the materials with complex structure in the case of ionic substitutions in the cation or anion sublattice. It is obvious that the doublets with different values of areas (Table IV) correspond to associates (clusters) with different percentage of Fe^{3+} ions in them and different environment of these ions in the nearest-neighbor cationic sphere.

On the basis of analysis of the parameters of spectra, the doublets due to Fe_1^{3+}, Fe_2^{3+}, Fe_3^{3+} may be attributed to the presence in $Zr_{0,886}Y_{0,057}Fe_{0,057}O_{2-\delta}$of sites of $Fe^{3+}$with the coordination number of six (IS = 0.63–0.66; QS = 0.84–1.33), five (IS = 0.49–0.52; QS = 0.92–0.94) and four (IS = 0.40–0.43; QS = 0.40–0.43) respectively (Table IV). It is evident that decrease in the coordination number of Fe^{3+} ions as compared with that of the cations in the basic structure Y-ZrO_2 (*c*, *t*-ZrO_2, CN 8; *m*-ZrO_2, CN 7) aids stabilization of the high-temperature zirconium dioxide modifications and exclusion or considerable retardation (depending on the Zr/Y/Fe ratio) of the low-temperature degradation of the structure due to the enhancement of Me–O bond energy.

The cationic composition of the samples under investigation calculated with allowance for the real iron content of them according to MS data (Table IV) was used in refining the oxygen site occupancy by the Rietveld analysis (Table II). The actual composition of the samples obtained by CPH and SPH corresponds to the formulas $Zr_{0.926}Y_{0.058}Fe_{0.016}O_{1.80}(V_O)_{0.20}$ and $Zr_{0.925}Y_{0.058}Fe_{0.017}O_{1.87}(V_O)_{0.13}$ respectively (where V_O = oxygen vacancies). The larger oxygen content and the higher value of lattice microstrain (η) in the samples obtained by SPH in comparison with the samples obtained by CPH (Table III) may be due to the fact that on SPH finer powders with more extended surface are formed (Fig. 4), which facilitates oxygen adsorption. This agrees with the results obtained in [26], where it was shown that the sample oxidizes and the oxygen vacancies are filled on annealing ZrO_2 vacancies in air or on cooling samples.

4. Conclusion

The polymorphic composition of a ZrO_2-based materials has been determined in series of samples that correspond to the formula $[1-(x+y)]ZrO_2 \cdot xY_2O_3 \cdot yFe_2O_3$

in the temperature range 620–1570 K. It has been found that at the same molar ratio ZrO_2 : doping oxides, the degree of ZrO_2 stabilization increases, and the low-temperature degradation process is retarded by the partial substitution of Fe^{3+} for Y^{3+}. Nonequivalent sites of Fe^{3+} ions have been identified: two with octahedral coordination for CPH and three with octa-, penta- and tetrahedral coordination for SPH. The possibility of cluster distribution of Fe^{3+} ions and the dependence of the number of vacancies on synthesis conditions have been shown.

References

1. I. V. DEDOV, V. A. KONASOV, V. A. MATYUKHA and A. I. SOLOVYOV, "Materials and Nanostructures: Production, Properties, Applications," in: Proceedings of An Interregional Conference with Foreign Participants (Krasnoyarsk, 1996) p. 126.
2. O. VASYLKIV and Y. SAKKA, *J. Amer. Ceram. Soc.* **84**(11) (2001) 2489.
3. V. V. VIKTOROV and A. A. FOTIEV, *Inorg. Mater.* **29**(9) (1993) 1254.
4. F. F. LANGE, G. L. DUNLOP and B. I. DAVIS, *J. Amer. Ceram. Soc.* **69**(3) (1986) 237.
5. T. T. LEPISTO and T. A. MANTYLA, *Ceram. Eng. Sci. Prod.* **10**(7–8) (1989) 1362.
6. A. G. BELOUS, Y. V. PASHKOVA, A. N. MAKARENKO, B. S. KHOMENKO and I. Y. PISNCHAI, *Inorg. Mater*. **33**(12) (1997) 1469.
7. V. G. PEICHEV, S. Y. PLINER and A. A. DOBIZHA, *Steklo i Keramika* (3) (1991) 26.
8. H. YANAGIDA, Metallurgia, Moscow (1986) p. 279.
9. Certificate of Analysis. Standard Reference Material 1976, Instrument Sensitivity Standard for X-ray Powder Diffraction (Gaithersburg: National Institute of Standards and Technology, 1991) p. 1–4.
10. T. V. CHUSOVITINA, Y. S. TOROPOV and M. G. TRETNIKOVA, *Ogneupory* (8) (1991) 14.
11. Y. N. KNIPOVICH and Y. V. MARACHEVSKII, Gosud. Nauchno-Tekhnich. Izdatelstvo Khim. Literatury, Leningrad, (1956) p. 1055.
12. Reagents. Chelatometric method for the determination of main-substance content, GOST 10398-76, Moscow, 1976.
13. V. P. CHALYI, Naukova Dumka, Kyiv (1972) p. 153.
14. A. N. MAKARENKO, A. G. BELOUS and Y. V. PASHKOVA, *J. Europ. Ceram. Soc*. **19** (1999) 945.
15. G. TEUFER, *Acta Cryst.* **15** (1962) 1187.
16. C. J. HOWWARD, R. J. HILL and B. E. REICHERT, *ibid.* **44** (1988) 116.
17. O. C. KISTNER and A. W. SUNYAR, *Phys. Rev. Letters.* **4**(8) (1960) 412.
18. G. SHIRANE, D. E. COX and S. L. RUBY, *Phys. Rev.* **125**(4) (1962) 1158.
19. F. N. RUBY and V. Y. ARSENIN, Nauka, Moscow (1979) p. 285.
20. G. BENCROFT, A. MEDDOK and R. BERNS, in "Fizika Mineralov," Mir, Moscow (1971) p. 179.
21. G. BENCROFT, R. BERNS and A. STONE, in "Fizika Mineralov," Mir, Moscow (1971) p. 205.
22. R. D. SHANNON and C. T. PREWITT, *Acta Cryst.* **B25** (1969) 925.
23. G. A. OLKHOVIK, I. I. NAUMOV, O. I. VELIKOKHATNYI and N. N. APAROV, *Inorg. Mater.* **29**(5) (1993) 636.
24. F. J. BERRY, M. H. LORETTO and M. R. SMITH, *J. Solid State Chem.* **83**(1) (1989) 91.
25. D. A. ZYUZIN, E. M. MOROZ, A. S. IVANOVA and V. I. ZAIKOVSKII, *Inorg. Mater.* **36**(4) (2000) 447.
26. A. P. SHPAK, Y. A. KUNITSKII and Z. A. SAMOILENKO, Akademkniga, Kyiv (2002) p. 167.

Received 28 October 2004
and accepted 7 March 2005